

Electronic Supplementary Information (ESI)

A luminescent metal–organic framework demonstrating ideal detection ability for nitroaromatic explosives

Dan Tian, Yue Li, Rong-Ying Chen, Ze Chang*, Guan-Yao Wang and Xian-He Bu

Table S1. Crystal data and structure refinement details for **1**^a.

Formula	C ₄₀₂ H ₃₃₈ N ₂ O ₁₁₆ Cd ₁₇
Fw	8963.54
Crystal system	trigonal
Space group	<i>R</i> 3 <i>c</i>
<i>a</i> (Å)	25.7369(5)
<i>b</i> (Å)	25.7369(5)
<i>c</i> (Å)	61.601(2)
α (°)	90
β (°)	90
γ (°)	120
<i>V</i> (Å ³)	35336.9(15)
<i>Z</i>	3
μ (mm ⁻¹)	0.821
<i>D_c</i> (g/cm ³)	1.264
<i>R</i> (int)	0.0657
GOF on <i>F</i> ²	1.026
<i>R</i> _{<i>I</i>} ^a [<i>I</i> > 2σ(<i>I</i>)]	0.0492
<i>wR</i> ₂ ^b [<i>I</i> > 2σ(<i>I</i>)]	0.1254

^a $R_I = \sum ||F_o| - |F_c|| / \sum |F_o|$; ^b $wR_2 = [\sum [w(F_o^2 - F_c^2)^2] / \sum w(F_o^2)^2]^{1/2}$.

Table S2. Bond lengths [Å] and angles [°] for complex **1^a**.

Cd(1)-O(4)#1	2.185(4)	Cd(1)-O(19)	2.236(2)
Cd(1)-O(3)#2	2.306(4)	Cd(1)-O(9)	2.340(4)
Cd(1)-O(10)	2.383(4)	Cd(1)-O(6)#3	2.455(3)
Cd(2)-O(5)#6	2.236(3)	Cd(2)-O(11)#7	2.253(4)
Cd(2)-O(20)	2.2751(12)	Cd(2)-O(6)#3	2.337(3)
Cd(2)-O(10)	2.347(4)	Cd(2)-O(12)#7	2.452(4)
Cd(3)-O(2)	2.264(3)	Cd(3)-O(21)	2.290(11)
Cd(3)-O(1)	2.528(3)	Cd(4)-O(1)	2.345(3)
Cd(4)-O(7)	2.347(3)	Cd(5)-O(7)	2.509(3)
Cd(5)-O(8)	2.275(3)	Cd(5)-O(1W)	2.260(12)
O(4)#1-Cd(1)-O(19)	114.05(12)	O(4)#1-Cd(1)-O(3)#2	112.54(16)
O(19)-Cd(1)-O(3)#2	83.36(15)	O(4)#1-Cd(1)-O(9)	95.05(15)
O(19)-Cd(1)-O(9)	148.70(13)	O(3)#2-Cd(1)-O(9)	96.39(14)
O(4)#1-Cd(1)-O(10)	146.18(14)	O(19)-Cd(1)-O(10)	92.98(11)
O(3)#2-Cd(1)-O(10)	89.49(13)	O(9)-Cd(1)-O(10)	55.75(12)
O(4)#1-Cd(1)-O(6)#3	90.95(14)	O(19)-Cd(1)-O(6)#3	81.90(15)
O(3)#2-Cd(1)-O(6)#3	155.86(13)	O(9)-Cd(1)-O(6)#3	86.55(13)
O(10)-Cd(1)-O(6)#3	72.35(12)	O(5)#6-Cd(2)-O(11)#7	102.09(16)
O(5)#6-Cd(2)-O(20)	99.15(10)	O(11)#7-Cd(2)-O(20)	136.85(16)
O(5)#6-Cd(2)-O(6)#3	153.89(13)	O(11)#7-Cd(2)-O(6)#3	92.06(16)
O(20)-Cd(2)-O(6)#3	84.60(12)	O(5)#6-Cd(2)-O(10)	82.31(13)
O(11)#7-Cd(2)-O(10)	92.61(14)	O(20)-Cd(2)-O(10)	127.36(17)
O(6)#3-Cd(2)-O(10)	75.15(12)	O(5)#6-Cd(2)-O(12)#7	105.55(16)
O(11)#7-Cd(2)-O(12)#7	54.58(15)	O(20)-Cd(2)-O(12)#7	83.70(18)
O(6)#3-Cd(2)-O(12)#7	100.54(16)	O(10)-Cd(2)-O(12)#7	147.05(14)
O(2)#4-Cd(3)-O(2)#5	120.000(2)	O(2)-Cd(3)-O(21)	99.9(3)
O(2)-Cd(3)-O(21)#5	86.6(5)	O(2)-Cd(3)-O(21)#4	83.8(3)
O(2)#4-Cd(3)-O(1)#5	89.48(13)	O(2)#5-Cd(3)-O(1)#4	126.37(12)
O(1)#5-Cd(3)-O(1)#4	72.40(11)	O(2)-Cd(3)-O(1)	53.97(12)
O(21)#5-Cd(3)-O(1)	137.8(5)	O(21)-Cd(3)-O(1)	144.1(5)
O(21)#4-Cd(3)-O(1)	127.6(3)	O(1)#5-Cd(4)-O(1)#4	79.10(12)
O(1)-Cd(4)-O(7)	153.03(11)	O(1)#4-Cd(4)-O(7)#5	88.33(10)
O(1)#5-Cd(4)-O(7)#4	122.08(11)	O(7)#5-Cd(4)-O(7)#4	78.22(12)
O(1W)-Cd(5)-O(8)	89.02(9)	O(8)#4-Cd(5)-O(8)#5	119.971(6)
O(1W)-Cd(5)-O(7)	137.05(7)	O(8)-Cd(5)-O(7)	55.27(11)
O(8)#4-Cd(5)-O(7)#5	127.58(12)	O(8)#5-Cd(5)-O(7)#4	89.86(12)
O(7)#5-Cd(5)-O(7)#4	72.32(11)		

^a symmetry codes: #1 $x+2/3, y+1/3, z+1/3$; #2 $-y+5/3, x-y+1/3, z+1/3$; #3 $x+1/3, x-y+2/3, z+1/6$; #4 $-y+1, x-y, z$; #5 $-x+y+1, -x+1, z$; #6 $-x+y+4/3, y-1/3, z+1/6$; #7 $-x+y+5/3, y+1/3, z-1/6$.

1. Synthesis of 2,4,6-tris[1-(3-carboxylphenoxy)ylmethyl]mesitylene (**H₃L**)

2,4,6-tris[1-(3-carboxylphenoxy)ylmethyl]mesitylene was prepared according to literature procedure.^{S1} In a typical reaction, a mixture of methyl 3-hydroxybenzoate (13.69 g, 0.09 mol), KI (148.0mg, 0.89 mmol), K₂CO₃ (42.0 g, 0.303 mol) and 1,3,5-tris(bromomethyl)-2,4,6-trimethylbenzene (5.98 g, 0.015mol) in DMF (400mL) was heated to 100 °C for 2 hours. The reaction mixture was cooled to room temperature and then poured into water to produce a white precipitate. The obtained solid was dissolved in methanol, and a solution of NaOH in H₂O was added. This mixture was refluxed for 12 h. After cooling down to room temperature, the solution was acidified to pH = 1 using concentrated HCl (15N). The precipitate was separated by filtration, washed with H₂O and air-dried to yield 10.0 g.

2. Solvent-dependent luminescence

The fine grinding sample **1** (3 mg) was immersed in different organic solvents (3mL), treated by ultrasonication for 30 min and then aged for 3 days to form a stable emulsion. The used solvents are alcohols (methanol, ethanol, 1-propanol, and 2-propanol), ketones (acetone), amides (DMF, DMAC), ethers (THF), chloroalkanes (ClCH₂CH₂Cl, CHCl₃, CCl₄), and even aromatic complex (benzene, toluene, nitrobenzene). As shown in Fig. S8a, the emission spectra of emulsions reveal maximum emission around 360 nm ($\lambda_{\text{ex}} = 290$ nm). The other primary feature is that the intensities of the emission spectra are largely dependent on the solvent molecules (Fig. S8b), particularly in the case of nitrobenzene, which exhibited the most quenching behavior.

3. The luminescence sensing of complex **1** on metal ions

Though our research interest focused on the detecting of nitrobenzene and similar pollutions and explosives, additional experiments were performed to preliminarily investigate the potential of this MOFs in ion sensing. Cu²⁺, Fe²⁺, Fe³⁺, Co²⁺, Ni²⁺ and Mn²⁺ (metal chloride) were tested (Fig. S9). The fluorescence spectroscopic studies were carried out with the

addition of 100 ppm different metal chloride. As shown in Fig. S9, Fe^{2+} , Fe^{3+} ions can nearly completely quenched the fluorescence of **1**, Cu^{2+} , Ni^{2+} ions exhibit comparable quenching capability with nitrobenzene, while Mn^{2+} , Co^{2+} ions show weaker quenching capability compared with nitrobenzene. However, the sensing of complex **1** on these ions exhibits low selectivity.

S1 J. F. Eubank, H. Mouttaki, A. J. Cairns, Y. Belmabkhout, L. Wojtas, R. Luebke, M. Alkordi and M. Eddaoudi, *J. Am. Chem. Soc.*, 2011, **133**, 14204.

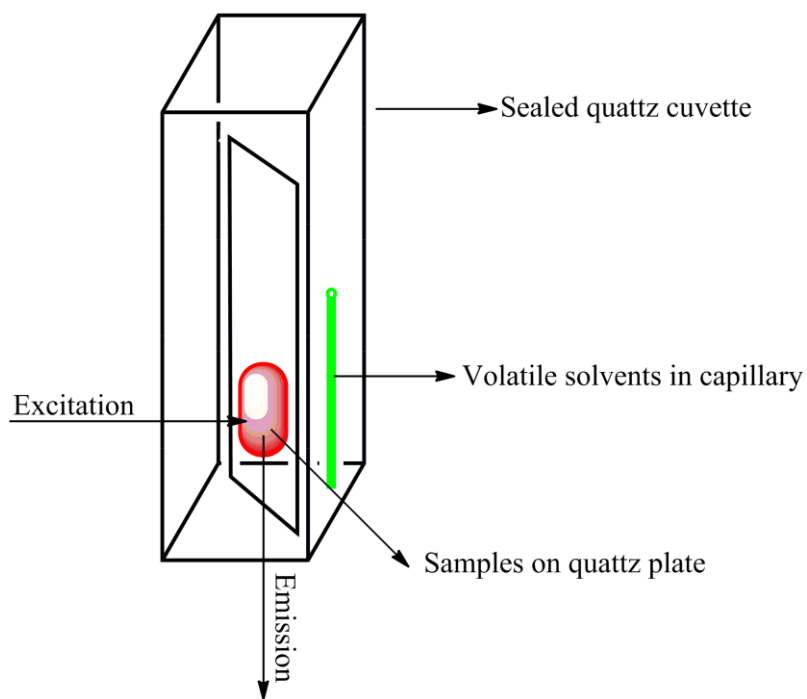


Figure S1. Experimental setup for the solid-gas detection of nitrobenzene vapour.

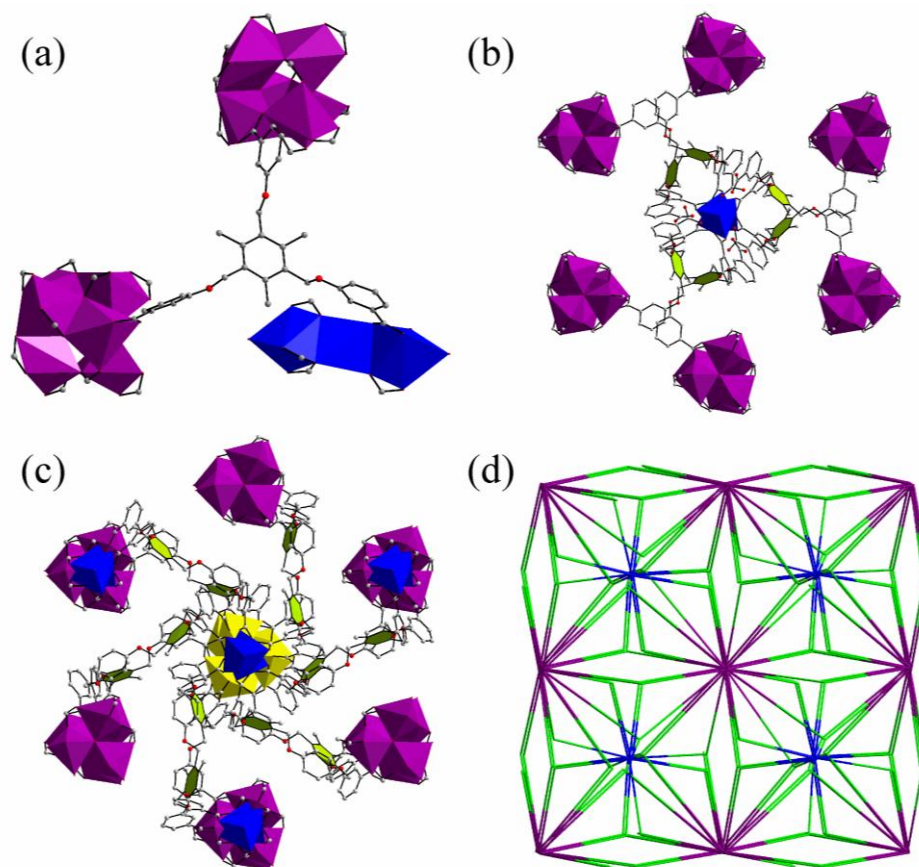


Figure S2. Schematic representations of the 3 (a), 6 (b), 12 (c) -connected nodes. (d) Schematic illustration of sqc-2585 topology of the 3D network of **1**.

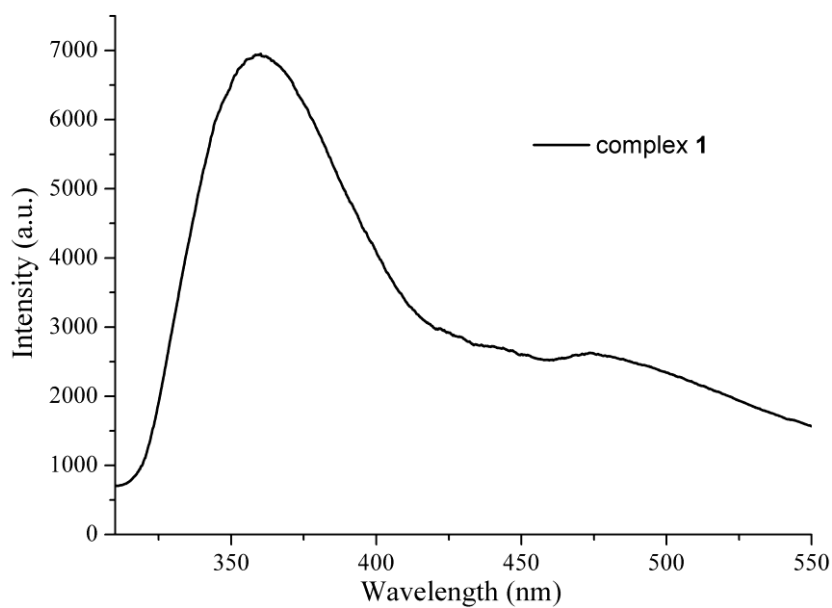


Figure S3. Solid-state emission spectra of **1** ($\lambda_{\text{ex}} = 290$ nm).

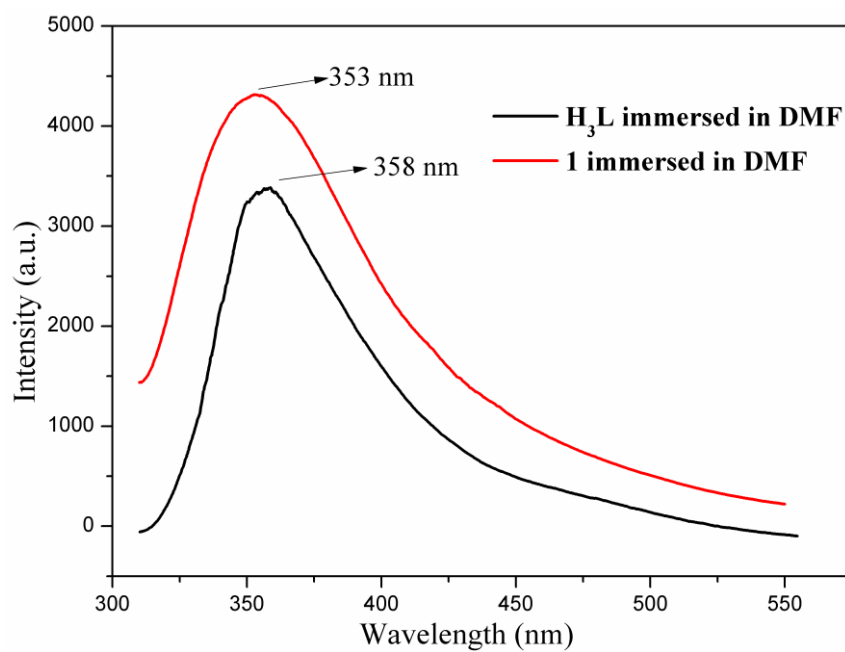


Figure S4. Liquid-state emission spectra of **1** and H₃L immersed in DMF ($\lambda_{\text{ex}} = 290$ nm).

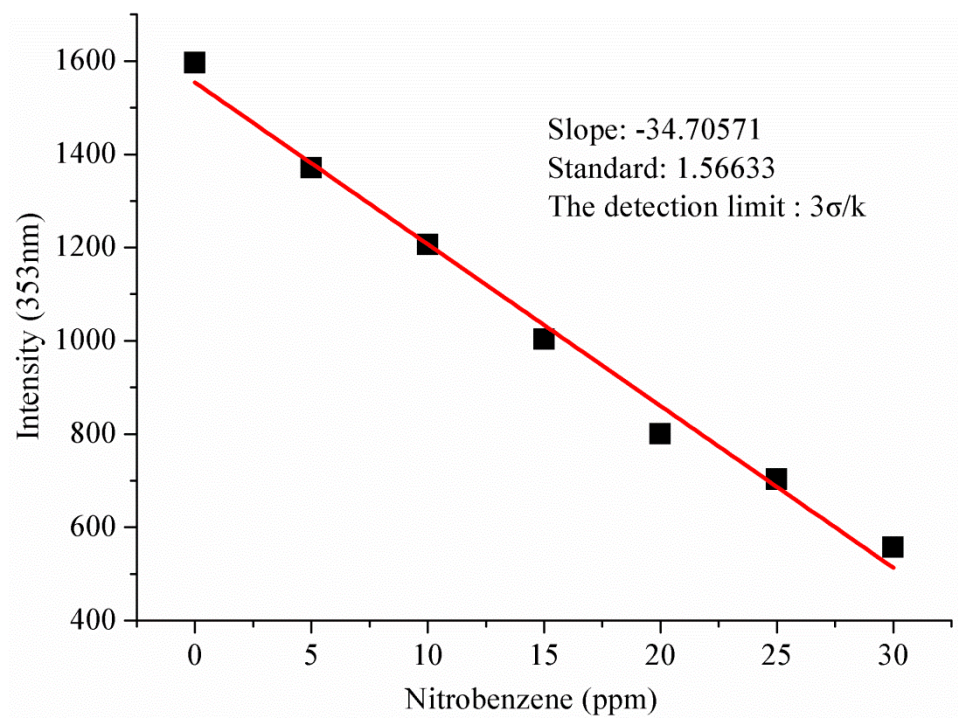


Figure S5. The detection limit 0.135 ppm was calculated with $3\sigma/k$ (k : slope, σ : standart) with a linear fitting range from 0 ppm to 30 ppm.

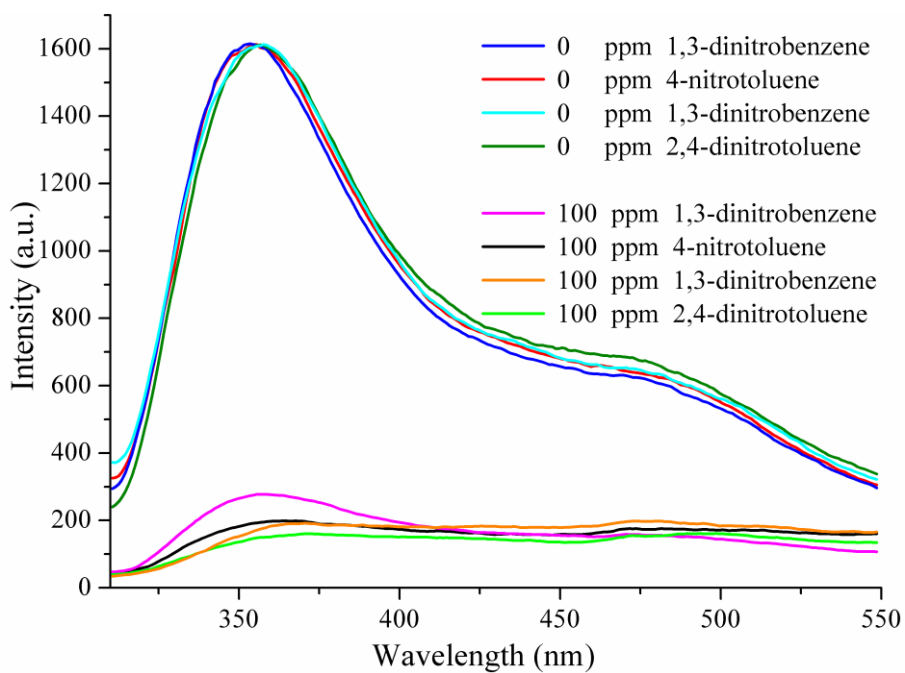


Figure S6. Emission spectra of **1** (3 mg) dispersed in 3 mL DMF with the addition of 100 ppm different nitro-containing complexes.

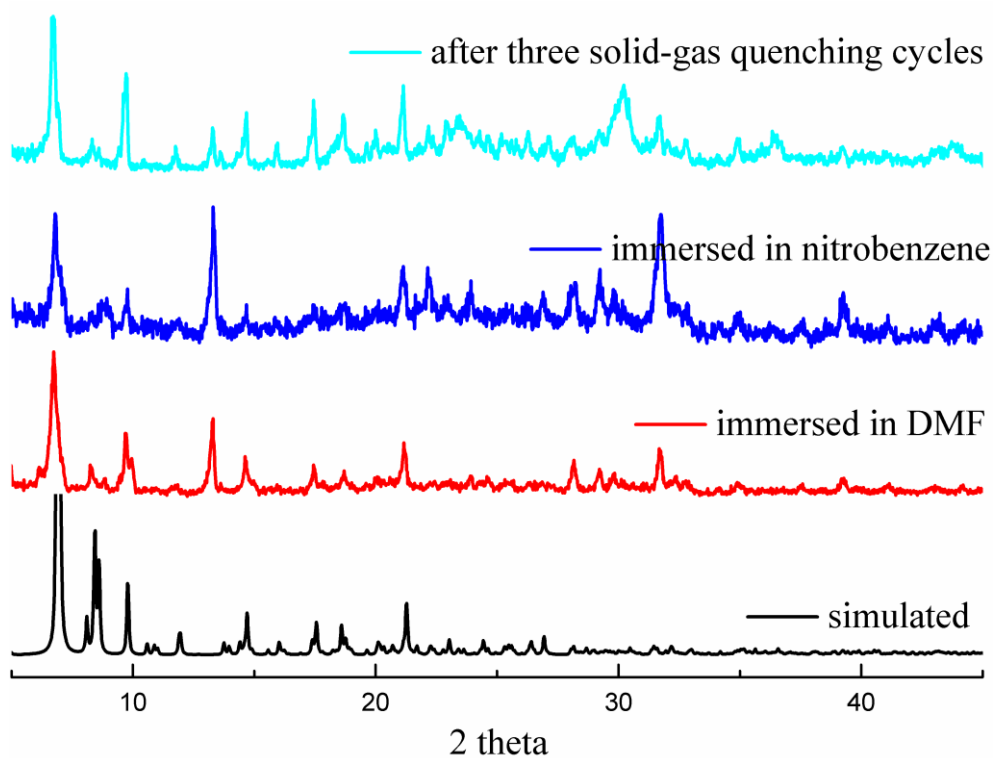


Figure S7. The XRPD patterns of complex **1**: the samples after three solid-gas quenching cycles (cyan), immersed in nitrobenzene (blue), immersed in DMF (red) and the simulated patterns based on X-ray single-crystal data (black).

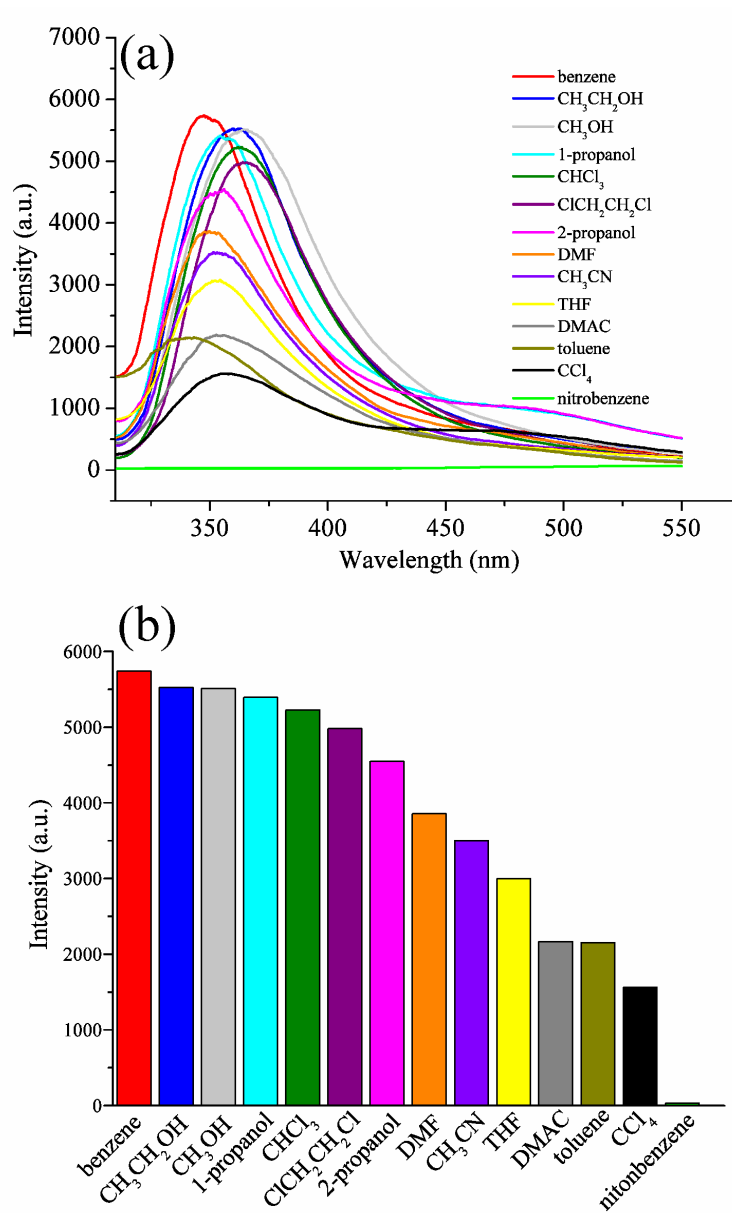


Figure S8. Emission spectra (a) and emission intensities (b) of **1** in different solvents when excited at 290 nm.

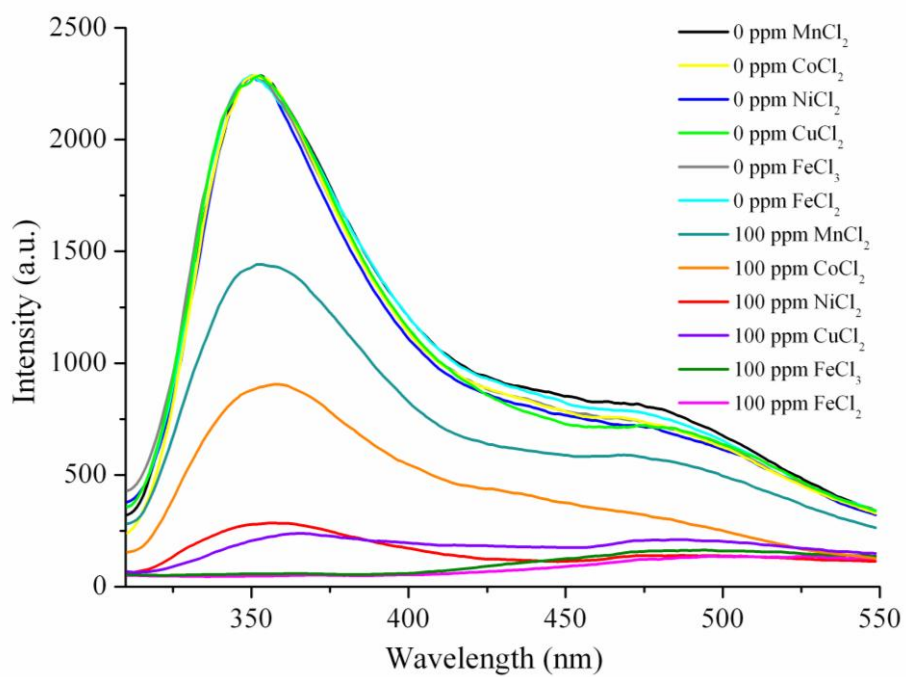


Figure S9. Emission spectra of **1** (3 mg) dispersed in 3 mL DMF with the addition of 100 ppm different metal chloride.

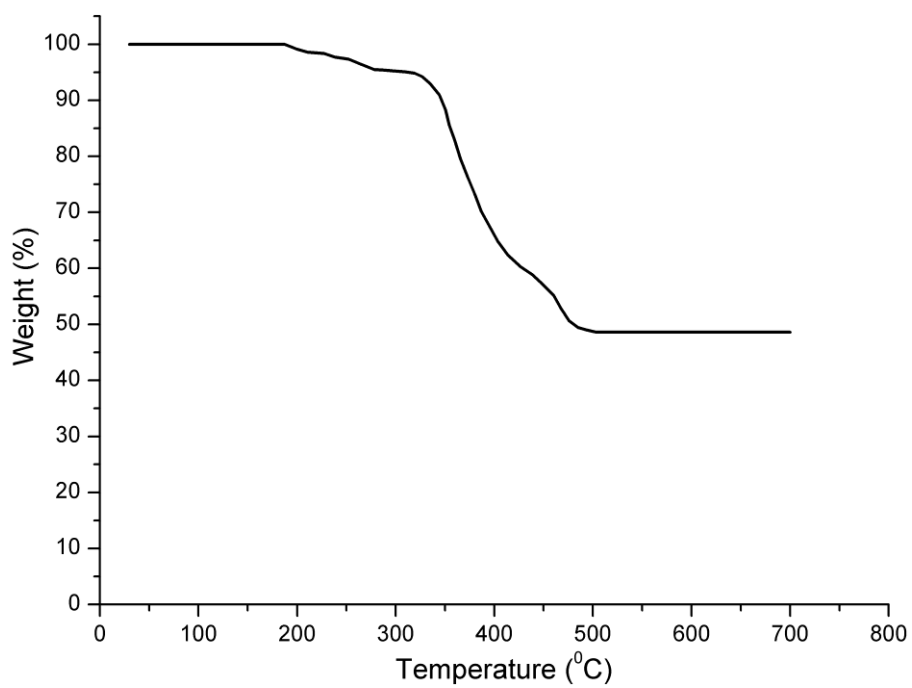


Figure S10. Thermogravimetric curve of complex 1.

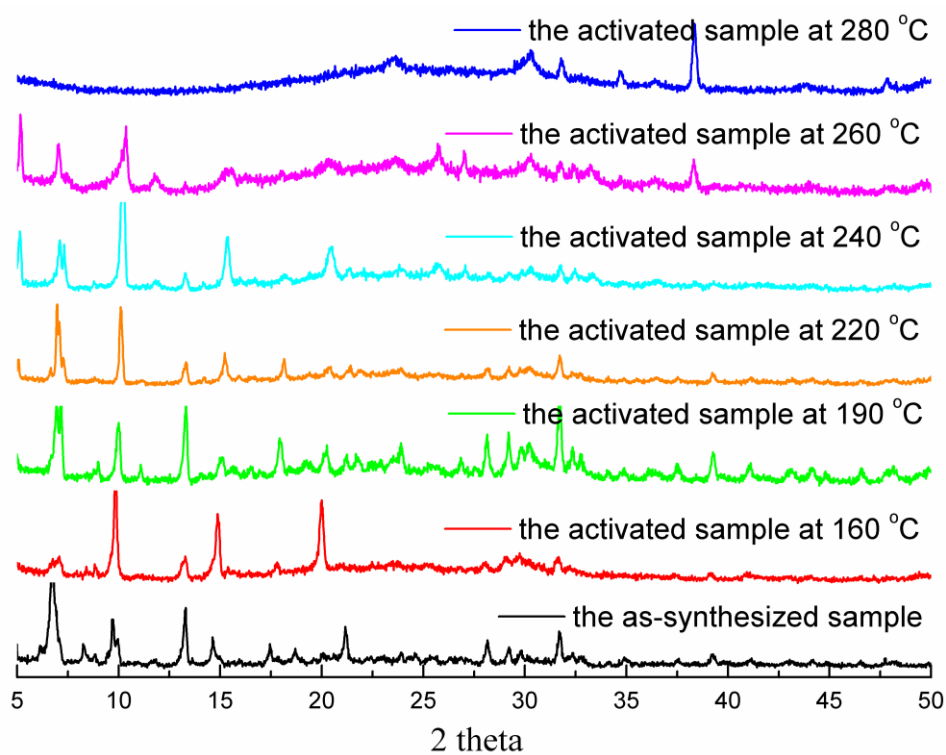


Figure S11. The XRPD patterns of complex **1**: the samples activated at 160, 190, 220, 240, 260, 280 °C, and the as-synthesized patterns based on X-ray single-crystal data.

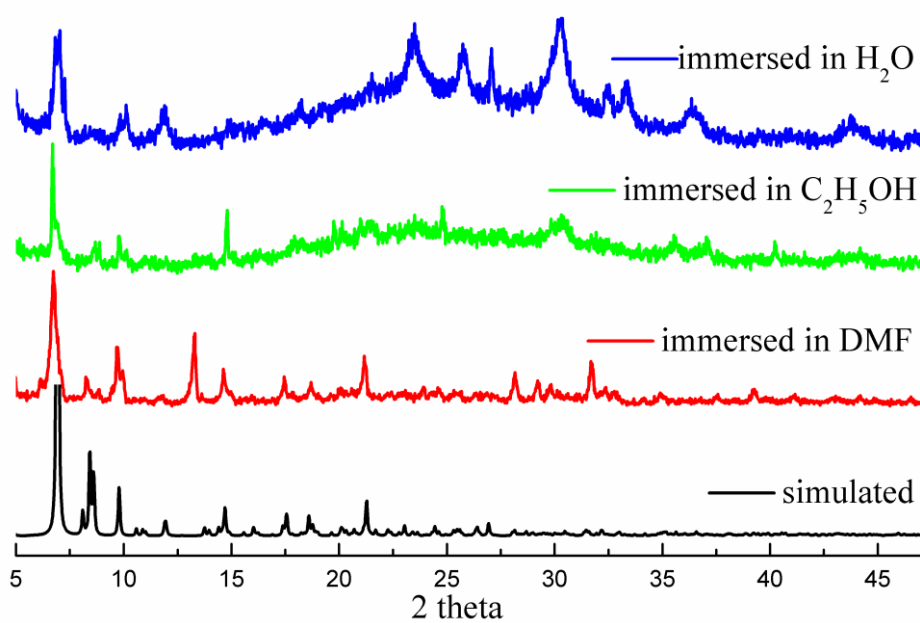


Figure S12. The XRPD patterns of complex 1: the samples immersed in H_2O (blue), immersed in $\text{C}_2\text{H}_5\text{OH}$ (green), immersed in DMF (red) and the simulated patterns based on X-ray single-crystal data (black).

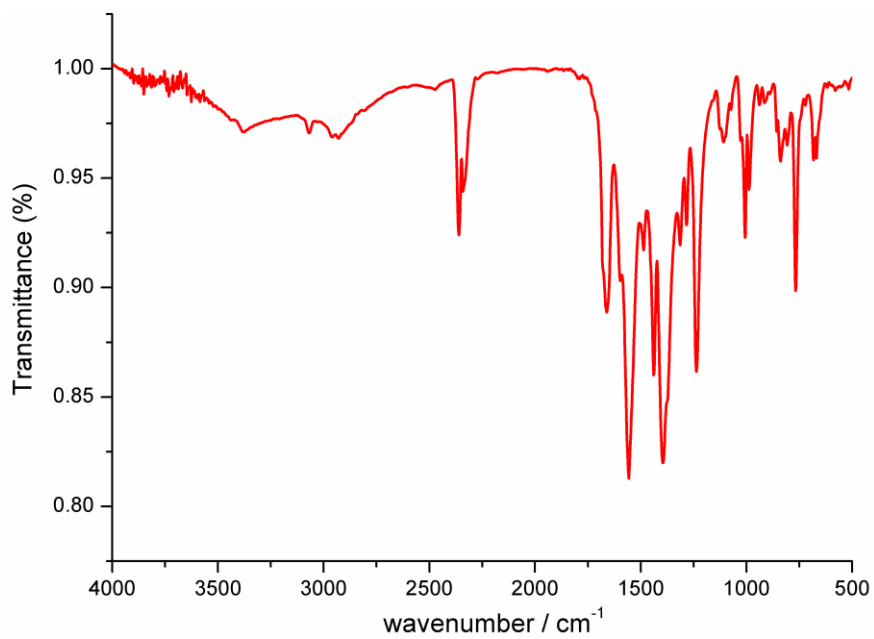


Figure S13. IR spectrum of complex **1**.